Supplementary Information

Cysteine-Rich Peptide for Chiral Self-Assembly: A Multi-Functional Antioxidant with Novel SH-Mediated ROS-Responsive Disassembly from Natural Medicine

Xiaohui Zhang[a], Zhuo Cao[a], Runkun Zhao[a], Youyou Guo[a], Jiahui Ren[a], Zhenbang Sun[a], Runhan Ye[a], Jun He[a], Yiyun Chen[a], Susanne K. Wiedmer[b], Qi Qin[c], Mengsui Zhou[a], Run Shi[d], Bingqing Yi[e*], Guodong Zhao[a,f*]

[a] *School of Chinese Materia Medica, Beijing University of Chinese Medicine, Beijing 102488, China*

[b] *Department of Chemistry, University of Helsinki, Helsinki, Finland*

[c] *Department of Neurology & Innovation center for neurological disorders, Xuanwu Hospital, Capital Medical University, Beijing, 100029, China*

[d] *Qi-Huang Chinese Medicine School, Beijing University of Chinese Medicine, Beijing 102488, China*

[e] *School of Life Sciences, Beijing University of Chinese Medicine, Beijing 102488, China*

[f] *Engineering Research Center for Pharmaceutics of Chinese Materia Medica and New Drug Development, Ministry of Education, Beijing, 100029, China*

[*] Corresponding author at: School of Chinese Materia Medica, Beijing University of Chinese Medicine, Beijing 102488, China (G. Zhao)

E-mail addresses: 202001036@bucm.edu.cn (G. Zhao), bingqingyi@126.com (B. Yi).

Table of Contents

1.	Materials and methods	P2
2.	Supplementary information for result and discussion	P10
3.	Reference	P37

1. Materials and Methods

1.1 Materials and Reagents

The photograph presented herein (Fig. S1) documents the original pangolin scale reference material (voucher no. 121027; batch no. 121027-201305) obtained from the National Institutes for Food and Drug Control (NIFDC, China), thereby confirming its authenticated origin and its exclusive use for analytical and research purposes.

Fig. S1. Authenticated pangolin (*Manis pentadactyla*) scale (PS) reference materials obtained from the NIFDC of China.

This work does not advocate the use of pangolin-derived materials; instead, it seeks to elucidate the structure and function of bioactive components from natural sources in order to inform the development of sustainable and ethically acceptable alternatives. Such efforts are intended to reduce reliance on endangered species and to facilitate the transition toward fully synthetic, controllable, and scalable bioactive systems.

Cell Counting Kit-8 (CCK-8) and assay kits for superoxide dismutase (SOD), catalase (CAT), glutathione peroxidase (GSH-Px) and malondialdehyde (MDA), and fresh rabbit blood were purchased from Shanghai Yuanye Biotechnology Co., Ltd. (China). α-Glucosidase was purchased from Sigma-Aldrich (St. Louis, USA). All Fmoc-protected amino acids, 2,2-diphenyl-1-picrylhydrazyl (DPPH), fluorescein isothiocyanate (FITC), 2,7-dichlorodihydrofluorescein diacetate (DCFH-DA) and other chemical reagent/dye were purchased from Anhui Zesheng Technology Co., Ltd. (China). HepG2 cell lines were purchased from the American Type Culture Collection (ATCC, USA). Wild type N2 *Caenorhabditis elegans* (*C. elegans*) and *Escherichia coli* OP50 (*E. coli* OP50) were provided by the Institute of Genetics and Developmental Biology, Chinese Academy of Sciences.

1.2 Generation of Bioaccessible Peptides with Enhanced Digestive Stability and

Absorption Potential

PS were ground into powder and degreased by petroleum ether to remove lipid impurities. The degreased powder was hydrolyzed using a pepsin-trypsin dual-enzyme system at 37°C to simulate human gastrointestinal digestion. Detailed hydrolysis conditions were optimized through a Box-Behnken design (three variables, three levels; Tables S1–S2, SI). The enzymatic hydrolysis was terminated by boiling, and the supernatant was freeze-dried, followed by ultrafiltration (<5 kDa) and Sephadex G-25 chromatography. Pangolin scale peptide (PSP) fractions were collected based on UV absorbance at 214 nm.

1.3 De Novo Sequencing and Structure Verification of the PSP

PSP mixture (1 mg) were subjected to standard de novo sequencing workflows, including desalting and reductive alkylation by iodoacetamide. Then the mixture was injected into nanoflow UHPLC system (Vanquish^{TM} Neo, Thermo Scientific, USA) equipped with a nanoViper^{TM} C18 column (75 μm × 25 cm, 1.9 μm particle size). Mobile phases were composed of (A) 0.1% formic acid in water and (B) 0.1% formic acid in 80% acetonitrile, delivered at 300 nL/min, with the column maintained at 25°C. The gradient program was as follows: 4-8% B (0-2 min), 8-28% B (2-105 min), 28-40% B (105-120 min), 40-95% B (120-121 min), and 95% B (121-131 min). Peptides separated by nano liquid chromatography were analyzed immediately using an Orbitrap Exploris 480 mass spectrometer (Thermo Scientific, USA). Mass spectrometry analysis was performed in positive ion mode using data-dependent acquisition (DDA), with automatic switching between full-scan MS and MS/MS modes. The resulting Raw data files were analyzed by PEAKS Studio 10.6 software for de novo peptide sequencing.

Predicted sequences with de novo scores > 90 were evaluated for toxicity and sensitization using ToxinPred2.0 (https://webs.iiitd.edu.in/raghava/toxinpred2/batch.html) and AlgPred 2.0 (https://webs.iiitd.edu.in/raghava/algpred2/batch.html), respectively. A three-tiered filtering strategy (de novo score >90, non-toxicity, and non-allergenicity) was applied, and selected peptides were synthesized via a high-throughput protocol developed in our lab[1].

Synthesized peptides (standard references) were pooled and analyzed using the same nano

UHPLC-MS/MS system under identical conditions to the initial hydrolysate analysis for de novo sequencing. Retention times and MS/MS spectra were compared between the standard and predicted peptides to verify sequence accuracy. Mirror-mode images and fragment ion intensity scatter plots were generated for visual comparison. Cosine similarity metrics were calculated for extracted b- and y-type fragment ion intensity vectors to quantify MS/MS spectral similarity (equation 1).

$$Cosine\ Similarity = \frac{I \cdot II}{||I|| \cdot ||II||} = \frac{\sum_{i=1}^{n} I_i * II_i}{\sqrt{\sum_{i=1}^{n} (I_i)^2} * \sqrt{\sum_{i=1}^{n} (II_i)^2}} \qquad \text{(equation 1)}$$

where I denote the intensity of the backbone fragment ion (b/y ions) in the initial de novo sequencing spectrum, and II represents the intensity of the corresponding fragment ion in the standard reference.

1.4 High-Throughput Screening for Self-Assembling Peptide and Their Stimuli-responsive Properties

Structure-verified peptides were prepared via parallel synthesis and screened for gelation capability. The selected peptide candidate was dissolved in water or methanol (10 mM) and equilibrated under ambient conditions for seven days before characterization. Gel formation was assessed using an inversion test. The gel was mechanically disrupted by vortexing and then left undisturbed to rest. Injectability was assessed by extruding the gel through a syringe needle to form patterns.

1.5 Systematic in vitro Antioxidant Evaluation

The antioxidant capacity of PSP was evaluated using three comprehensive assays: (1) DPPH radical scavenging, (2) ABTS radical scavenging, and (3) ferricyanide reducing power assays.

1.6 Attenuated Total Reflectance-Fourier Transform Infrared Measurement (ATR-FTIR)

FTIR spectra were acquired using a Nicolet iS10 spectrometer (Thermo Fisher) in ATR mode with a diamond crystal. Gel solutions were applied to the crystal and dried to form thin films. Spectra were averaged from 24 scans at 4 cm^{-1} resolution, followed by background subtraction

and baseline correction.

1.7 Circular Dichroism (CD) Measurements

CD spectra were recorded using a Chirascan^{TM} V100 spectropolarimeter (Applied Photophysics, UK). Measurements used a 1 mm path-length quartz cuvette at 25°C. Spectra (270–190 nm) were acquired with 1 nm bandwidth, 1 nm step size, and 1 s integration time per point. Spectra were averaged from three scans and solvent-subtracted. Mean residue ellipticity ([θ], in deg·cm^2·dmol^{-1}) was calculated using equation 2.

$$[\theta] = \frac{\theta}{10lcN} \qquad \text{(equation 2)}$$

where θ is the measured ellipticity in mdeg, l is theoptical length in cm, c is the peptide molar concentration, and N is the number of peptide units in the peptide.

1.8 Scanning Electron Microscopy (SEM)

Gel solutions were deposited on freshly cleaved silicon wafers and dried under nitrogen flow, then sputter-coated with gold for conductivity, and imaged using a Hitachi SU8660 SEM (Hitachi High-Technologies Corporation, Japan) at 3.0 kV accelerating voltage.

1.9 Negative-stain Transmission Electron Microscopy (TEM)

TEM was conducted on a Talos F200X microscope (Thermo Fisher Scientific, USA) at 200 kV. Samples were prepared by depositing gel onto 300-mesh copper grids (5 min adsorption), blotted with filter paper, and negatively stained with 2% (w/v) phosphotungstic acid or uranyl acetate.

1.10 Atomic Force Microscopy (AFM)

AFM imaging was performed using a Bruker Multimode VIII system with Bioscope Catalyst (Bruker Nano, USA). Samples were prepared by depositing the gel onto freshly cleaved mica, dried under a nitrogen flow, and scanned at 1.50 Hz (0º scan angle).

1.11 In vivo Antioxidant Investigation of Pangolin Scale Peptide Gel by C. elegans

1.11.1 C. elegans Culture and Synchronization

Wild-type N2 strain was feeded with *E. coli* OP50 at 22℃ in nematode growth medium (NGM) plates. Synchronization was achieved by bleaching adult nematodes (0.4 M NaOH/1.25% NaClO). Nematodes were treated with lyophilized pangolin scale peptide Ac-KCSQLNVNCKG (PSPA) gel until they reach the L4 stage after synchronization. Triplicate plates (30 nematodes/plate) were prepared per group, with M9 buffer as control.

1.11.2 ROS Level Determination in C. elegans Using DCFH-DA Fluorescent Dye

Following 3-day treatment with/without lyophilized PSPA gel, nematodes were incubated with 10 μM DCFH-DA (1 mL) in the dark for 2 h, then washed with M9 buffer to remove unincorporated dye. After levamisole anesthesia, worms were mounted on 2% agar pads for fluorescence imaging (λ_{ex} = 470 nm, λ_{em} = 525 nm).

1.11.3 Detection of Lipofuscin Accumulation in C. elegans

After 5-day treatment with/without lyophilized PSPA gel, levamisole-paralyzed nematodes were mounted on 2% agar pads. Autofluorescence was quantified using a Nikon Ts2R microscope (λ_{ex} = 385 nm, λ_{em} = 430 nm) when fully extended.

1.11.4 Detection of Lipid Accumulation in C. elegans

Following 3-day treatment with/without lyophilized PSPA gel, worms were fixed in 4% paraformaldehyde and flash-frozen at -80°C (15 min). After centrifugation, samples were stained with Oil Red O (ORO; 1 h, dark). Unbound ORO was removed by sequential washes (60% isopropanol, then M9 buffer). For imaging, worms were mounted on 2% agar pads and imaged by bright-field microscopy.

1.11.5 Heat and Oxidative Stress Resistance Assays in C. elegans

After 3-day treatment with/without lyophilized PSPA gel, worms were subjected to 37°C heat stress (t = 0 h). For oxidative stress tests, treated nematodes were exposed to 240 μM juglone at 22°C. Survival was assessed hourly by tactile response until complete mortality.

1.11.6 Cell Apoptosis Assay in C. elegans

Apoptosis was evaluated in control and peptide gel-treated worms (3-day exposure) using acridine orange staining. After M9 washes, worms were stained with 250 μg/mL acridine orange (1 h, 25°C, dark). After staining, worms were washed three with M9 to remove excess dye, and observed by inverted fluorescence microscope (λ_{ex} = 488 nm, λ_{em} = 515 nm).

1.11.7 Antioxidant Enzymes Activities and MDA Level in C. elegans

Following 3-day treatment with/without lyophilized PSPA gel, nematodes were washed with M9 buffer. Lysates were prepared via ultrasonication in ice-cold lysis buffer (1 mL) and clarified by centrifugation. Using commercial kits, we quantified: (1) SOD/CAT/GSH-Px activities (U/mg protein) and (2) MDA content (nmol/mg protein). Protein concentrations were determined by bicinchoninic acid (BCA) assay (triplicate measurements).

1.12 Cellular Uptake Activity of Ac-KCSQLNVNCKG

1.12.1 Synthesis of FITC–peptide conjugate

The cell-penetrating activity of pangolin scale peptide Ac-KCSQLNVNCKG (PSPA) was assessed via fluorescein isothiocyanate (FITC) conjugation, using TAT peptide (RKKRRQRRR) as positive control[2]. FITC-labeled peptides were synthesized by solid-phase peptide synthesis[1]. 6-Aminohexanoic acid spacers were incorporated between peptides and FITC to prevent intramolecular cyclization and N-terminal degradation during acid cleavage[3].

1.12.2 Cell Culture and Peptide Uptake Assay

HepG2 cells were maintained in DMEM supplemented with 10% heat-inactivated fetal bovine serum (FBS) at 37°C with 5% CO_2 and subcultured every 48 hours. HepG2 cells were seeded in 24-well plates and cultured for 24 h. After serum starvation (2 h in serum-free DMEM), cells were treated with: (1) serum-free DMEM (blank), (2) 20 μM FITC-PSPA (test), or (3) 20 μM FITC-TAT (positive control). After 2 h, cells were counterstained with DAPI. FITC-peptide uptake (green, λ_{ex} = 488 nm/λ_{em} = 525 nm) was imaged by fluorescence

microscopy. Cell nuclei (blue, λ_{ex} = 358 nm/λ_{em} = 461 nm) served as spatial reference.

1.12.3 Flow Cytometric Analysis

The cell-penetrating capacity of FITC-peptide was quantified by flow cytometry in HepG2 cells. Cells (2×10^5/well in 6-well plates) were treated with FITC-peptide (20 μM, 2 h), washed with PBS and digested with 0.25% trypsin to collect the cells. Internalization was measured on a flow cytometer (488 nm laser; Thermo Fisher Scientific, USA). Data were analyzed in FlowJo software (v10.8.1), and the relative internalization degree was quantified by the mean fluorescence intensity (MFI) of the living cell population gated by forward scattering (FSC) and lateral scattering (SSC).

1.12.4 Cytotoxicity Test for PSPA

Cell viability was assessed using Cell Counting Kit-8 (CCK-8) assay. HepG2 cells were cultured for 24 hours to ensure full adhesion. After replacing medium with PSPA (20 μM) in fresh medium, cells were cultured for 24 h. CCK-8 reagent was added, followed by 2 h incubation (37°C, dark). Absorbance was measured at 450 nm using a microplate reader (BioTek, USA). Viability was normalized to untreated controls (100%).

1.13 α-Glucosidase Inhibitory in vitro and its Kinetic Analysis

1.13.1. α-Glucosidase Inhibitory Assay

In 96-well plates, α-glucosidase (0.1 U/mL in PBS, pH 7.0; 60 μL) was pre-incubated with PSPA (40 μL) for 10 min at 37°C. After adding *p*-nitrophenyl-*α*-D-glucopyranoside (4-*p*NPG; 2.5 mM, 60 μL) substrate, reactions proceeded at 37°C for 20 minutes before the absorbance at 405 nm was measured. The α-glucosidase inhibitory rate was calculated by equation3.

$$\text{inhibitory}\ (\%) = 1 - \frac{A_1 - A_0}{A_C - A_{bk}} \times 100\% \qquad \text{(equation 3)}$$

where A_1 is the absorbance of the experimental group, containing enzymes, tested compounds and substrates, and A_0 is the background group without enzymes. A_c represents the absorbance of the control group without samples, and A_{bk} is the blank control group without samples and enzyme.

1.13.2 Type of α-Glucosidase Inhibition by Kinetic Analysis

Reaction mixtures contained α-glucosidase with PSPA (0-0.4 mM) and 4-*p*NPG (0.5-5 mM) in PBS (pH 7.0). Kinetic analysis used Lineweaver-Burk plots (1/V vs 1/S), where V = reaction velocity and S = substrate concentration (equation 4). Linear regressions at varying PSPA determined inhibition type and kinetic constants.

$$\frac{1}{V} = \frac{1}{V_{max}} + \frac{K_m}{V_{max}} \times \frac{1}{S} \qquad \text{(equation 4)}$$

where K_m and V_{max} denote the Michaelis-Menten constant and maximum velocity, respectively. The kinetic parameters K_m and V_{max} were derived from the linear regression analysis of the Lineweaver-Burk plot's intercepts.

1.13.3 Molecular Docking

Molecular docking was performed with AutoDock Vina 1.1.2. The α-glucosidase structure (PDB: 3A4A) was downloaded from RCSB protein database (https://www.rcsb.org/). The peptide ligand was built in ChemDraw 19.0 and energy-minimized in Chem3D. The receptor (α-glucosidase) was kept rigid, while allowing full ligand flexibility during docking. The lowest-energy conformation was visualized in PyMOL 2.5 and Discovery Studio 4.0.

1.14 Hemocompatibility Evaluation of Peptide Gel

Rabbit blood was centrifuged, and the pelleted erythrocytes were washed three times with sterile, ice-cold PBS (10 mM, pH 7.4). A 2% (*v*/*v*) erythrocyte suspension was prepared. PBS and distilled water served as the negative and positive controls, respectively. Experimental groups contained PBS with varying PSPA gel concentrations (100–500 μM). After 1 h of incubation at room temperature, samples were vortexed, centrifuged, and the supernatant absorbance was measured at 540 nm. Hemolysis percentage was calculated using equation 5.

$$\text{Hemolysis rate} = \frac{A1-A0}{A2-A0} \times 100\% \qquad \text{(equation 5)}$$

where A1, A2, and A0 stand for the absorbance of samples, positive control, and negative control at 540 nm, respectively

1.15. Statistical Analysis

All experiments were performed in triplicate, with results expressed as mean ± standard deviation (SD). Data were analyzed using SPSS 19.0 (SPSS Inc., Chicago, IL, USA) and GraphPad Prism 8 (GraphPad Software Inc., San Diego, California USA). A one-way analysis of variance (ANOVA) and Duncan's multiple range test are used to analyze variance and means comparison by the use of SPSS software. Statistically significant differences were defined as $p < 0.05$.

2. Supplementary Information for Result and Discussion

2.1 Generation of Bioaccessible Peptides with Enhanced Digestive Stability and Absorption Potential

To obtain pangolin-derived peptide fragments with enhanced stability and bioavailability, defatted pangolin scales were sequentially hydrolyzed with pepsin and trypsin under simulated gastrointestinal conditions. This targeted proteolysis was designed to degrade labile regions, thereby enriching the hydrolysate for structurally stable peptides. Due to the study's focus on antioxidant properties, DPPH radical scavenging activity (DRSA) was selected as the response variable. Consequently, a systematic optimization study was conducted using three critical factors—pH, hydrolysis time, and enzyme-to-substrate ratio (E/S)—as independent variables. Response surface methodology (RSM) was applied to optimize hydrolysis parameters for maximal DRSA yield. The optimization ranges for each parameter (Tables S1–S2) were determined using defatted pangolin scales as the substrate.

Table S1 Box-Behnken response surface experiment factor level design for Pepsin

Level	Factors		
	pH value	Enzymatic hydrolysis time (h)	E/S (%)
-1	1	1	1
0	1.5	1.5	2
1	2	2	3

Table S2 Box-Behnken response surface experiment factor level design for Trypsin

Level	Factors		
	pH value	Enzymatic hydrolysis time (h)	E/S (%)
-1	7	2	1
0	7.5	2.5	2
1	8	3	3

A three-factor, three-level Box-Behnken design (BBD) was used to optimize pepsin hydrolysis conditions (Table S1), with pH (A: 1.0-2.0), hydrolysis duration (B: 1-2 h), and enzyme-to-substrate ratio (E/S, C: 1-3%) as independent variables. The results are presented in Table S3. And the DRSA was measured using a 3 mg/mL concentration of the enzymatic hydrolysate supernatant.

Table S3 Box-Behnken response surface experimental results for Pepsin

Experiment number	Enzymatic pH	Enzymatic hydrolysis time (h)	E/S (%)	DPPH scavenging rate (%)	Standard deviation
1	1	1	2	80.20	0.33
2	2	1	2	79.89	0.69
3	1	2	2	80.22	0.66
4	2	2	2	78.35	0.74
5	1	1.5	1	80.32	0.60
6	2	1.5	1	77.74	0.24
7	1	1.5	3	81.07	0.16
8	2	1.5	3	80.11	1.37
9	1.5	1	1	80.45	0.31
10	1.5	2	1	80.10	0.88
11	1.5	1	3	82.31	0.92
12	1.5	2	3	81.37	0.57
13	1.5	1.5	2	85.11	0.92
14	1.5	1.5	2	85.71	0.71
15	1.5	1.5	2	85.26	0.40
16	1.5	1.5	2	84.96	0.55
17	1.5	1.5	2	85.35	1.43

The DRSA of pangolin scale hydrolysates was chosen as the response variable. Using Design-Expert 12.0 software, a quadratic polynomial regression model was established as

follows:

$$Y = 85.28 – 0.7154A – 0.3504B + 0.7817C – 0.3904AB + 0.4038AC – 0.1472BC – 3.43A^2 – 2.18B^2 – 2.04C^2$$

where Y represents the DRSA (%), A represents the PH, B represents hydrolysis duration, and C represents the E/S ratio (%).

ANOVA results (Table S4) showed the regression model was highly significant ($p < 0.0001$). The model showed no significant lack of fit ($p = 0.4972$), confirming its adequacy for experimental analysis. Factor significance analysis revealed the following order of influence on DRSA: E/S ratio > pH > hydrolysis time. The high coefficient of determination ($R^2 = 0.9949$) indicated excellent predictive reliability. The adjusted R^2 (0.9884) confirmed model robustness, accounting for 98.84% of response variability (Table S4). The model effectively analyzes hydrolysis condition-DRSA correlations and demonstrates robust predictive performance.

Table S4 Response surface regression model ANOVA for Pepsin

Source of variance	Square sum	df	Mean square	F value	P value	Significance
Modelling	107.93	9	11.99	152.79	< 0.0001	significant
A – PH	4.09	1	4.09	52.17	0.0002	
B – Time	0.9823	1	0.9823	12.52	0.0095	
C - E/S	4.89	1	4.89	62.28	< 0.0001	
AB	0.6098	1	0.6098	7.77	0.027	
AC	0.6523	1	0.6523	8.31	0.0236	
BC	0.0866	1	0.0866	1.1	0.3283	
A^2	49.64	1	49.64	632.45	< 0.0001	
B^2	20.06	1	20.06	255.58	< 0.0001	
C^2	17.49	1	17.49	222.82	< 0.0001	
Residual	0.5494	7	0.0785			
Lack of Fit	0.2283	3	0.0761	0.9482	0.4972	not significant
Pure Error	0.3211	4	0.0803			
Cor Total	108.48	16				
R^2=0.9949	R^2_{adj}=0.9884					

The multivariate nonlinear regression equation generated RSM plots, with both 3D response surfaces and 2D contour plots clearly visualizing interactions between independent variables

(Figure S2). Elliptical contour plots indicate stronger interactions than circular ones[4]. Figures S2A-B reveal that both pH/(E/S) (AC) and pH/hydrolysis time (AB) interactions significantly influenced DPPH radical scavenging activity ($p < 0.05$), as evidenced by their elliptical contours and steep response surfaces. In contrast, Figure S2C's near-circular contours suggest a weaker E/S-hydrolysis time (BC) interaction, aligning with regression results in Table S4.

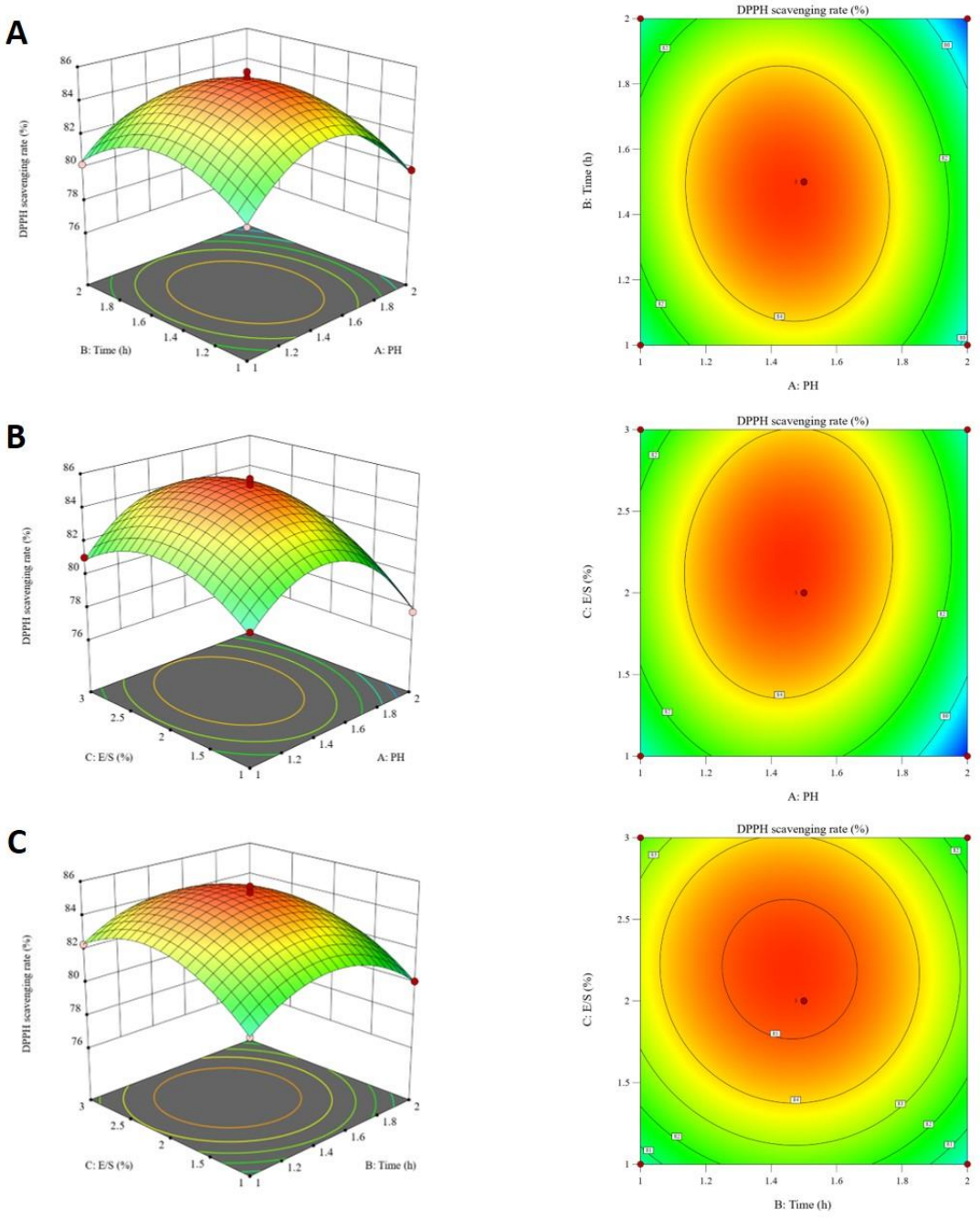

Fig. S2. 3D response surface and 2D contour plot of Pepsin to DRSA, interaction of pH, enzyme

addition, and hydrolysis time.

The model predicted optimal DPPH scavenging conditions as: pH 1.44, 1.45 h hydrolysis time, and 2.19% enzyme-to-substrate ratio, with 85.39% predicted activity. For practical implementation, hydrolysis was conducted at pH 1.4, 1.5 h duration, and 2.2% enzyme-to-substrate ratio. Experimental results (85.04% DRSA at 3 mg/mL hydrolysate concentration) agreed well with predictions (85.39%), validating the RSM model.

Parallel trypsin hydrolysis experiments were conducted using defatted pangolin scales as the substrate, with results presented in Tables S5-S6 and Figure S3.

Table S5 Box-Behnken response surface experimental results for Trypsin

Experiment number	Enzymatic pH	Enzymatic hydrolysis time (h)	E/S (%)	DPPH scavenging rate (%)	Standard deviation
1	7	2	2	50.62	0.77
2	8	2	2	49.81	0.28
3	7	3	2	50.07	1.14
4	8	3	2	48.33	0.72
5	7	2.5	1	50.60	1.57
6	8	2.5	1	47.85	0.28
7	7	2.5	3	51.27	0.42
8	8	2.5	3	50.86	2.89
9	7.5	2	1	50.41	1.13
10	7.5	3	1	50.13	1.07
11	7.5	2	3	52.22	2.11
12	7.5	3	3	51.61	0.51
13	7.5	2.5	2	55.58	2.85
14	7.5	2.5	2	55.30	1.01
15	7.5	2.5	2	55.67	0.42
16	7.5	2.5	2	55.54	1.09
17	7.5	2.5	2	55.46	0.51

Table S6 Response surface regression model ANOVA for Trypsin

Source of variance	Square sum	df	Mean square	F value	P value	Significance
Modelling	112.17	9	12.46	289.24	< 0.0001	significant
A - PH	4.09	1	4.09	94.95	< 0.0001	
B - Time	1.07	1	1.07	24.92	0.0016	

C - E/S	6.08	1	6.08	141.13	< 0.0001	
AB	0.2217	1	0.2217	5.15	0.0576	
AC	1.36	1	1.36	31.51	0.0008	
BC	0.0266	1	0.0266	0.6178	0.4577	
A^2	48	1	48	1113.97	< 0.0001	
B^2	24.79	1	24.79	575.38	< 0.0001	
C^2	16.7	1	16.7	387.63	< 0.0001	
Residual	0.3016	7	0.0431			
Lack of Fit	0.2263	3	0.0754	4.01	0.1066	not significant
Pure Error	0.0753	4	0.0188			
Cor Total	112.47	16				
R^2= 0.9973	R^2_{adj}= 0.9939					

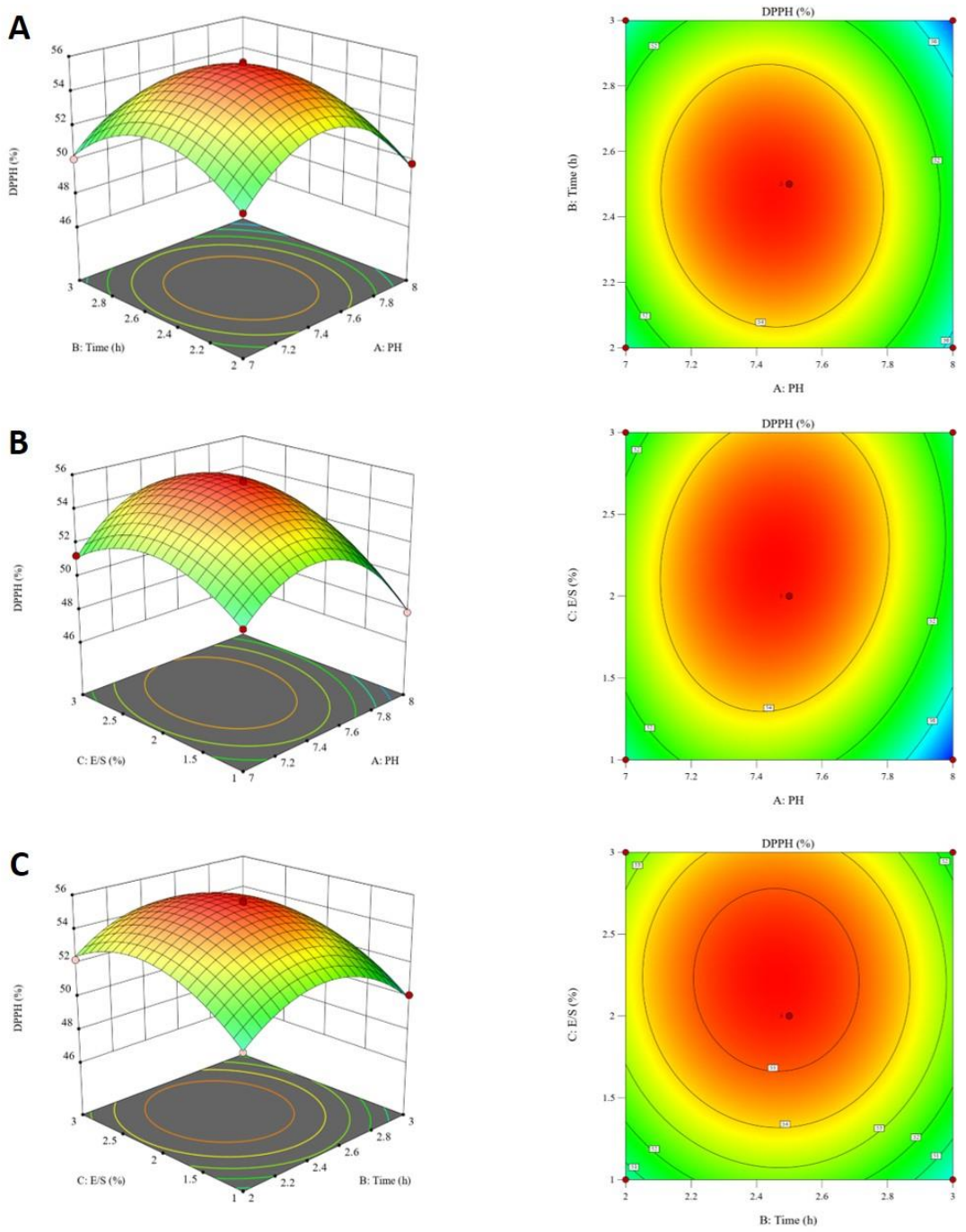

Fig. S3. 3D response surface and 2D contour plot of Trypsin to DRSA, interaction of pH, enzyme addition, and hydrolysis time.

The DRSA of pangolin scale hydrolysates was selected as the response variable. Using Design Expert 12.0 software, a quadratic polynomial regression model was established as follows:

$$Y = 55.51 - 0.7151A - 0.3663B + 0.8719C - 0.2355AB + 0.5826AC - 0.0816BC - 3.38A^2 - 2.43B^2 - 1.99C^2$$

where Y represents the DPPH radical scavenging rate (%), A represents the PH, B represents hydrolysis duration, and C represents the E/S ratio (%).

The model predicted optimal DPPH scavenging conditions as pH 7.43, 2.46 h hydrolysis duration, and 2.2% enzyme-to-substrate ratio, with a predicted DRSA of 55.63%. For practical implementation, trypsin hydrolysis was performed at pH 7.4 for 2.5 h with 2.2% enzyme-to-substrate ratio. The experimental DRSA (55.83% at 3 mg/mL) showed excellent agreement with the predicted value (55.63%), confirming the model's accuracy.

2.2 Enrichment of PSP from Human Gastrointestinal Hydrolysate

To isolate small-molecule fragments, the enzymatic solution was first filtered through a 5 kDa ultrafiltration membrane, yielding a <5 kDa fragment mixture. Subsequently, the peptide-containing solution was desalted and separated via Sephadex G-25 gel filtration chromatography, with UV detection at 214 nm to target peptide bonds. Based on the UV detection profile, two primary mixtures, designated S1 and S2, were isolated from the eluate (Fig. S4). These components likely represent peptide mixtures with distinct molecular weights or properties. For comprehensive analysis of pangolin scale peptide (PSP) digested by human gastrointestinal enzymes, S1 and S2 were pooled for nano UPLC-MS/MS analysis (Fig. S4).

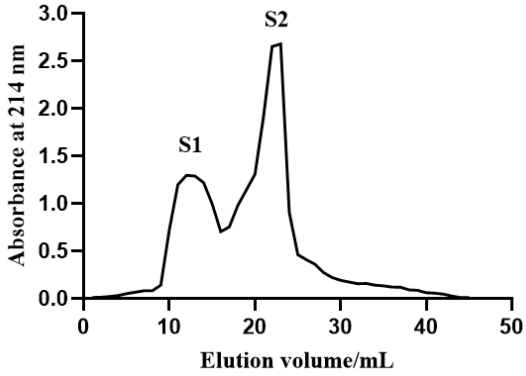

Fig. S4. SephadexG-25 chromatographic elution diagram of pangolin scale hydrolysate at an absorbance of 214 nm.

2.3 Screening Criteria for the De Novo Predicted Peptide Sequences

Based on the UPLC-MS/MS analysis and subsequent de novo sequencing via peptidomics, we predicted a substantial number of peptide sequences derived from pangolin scales. To

maximize prediction accuracy and eliminate potentially toxic and immunogenic side effects, we applied stringent screening using the following three specific criteria:

1) de novo score > 90. The de novo scoring system, which ranges from 1 (low confidence) to 99 (high confidence), reflects the algorithm's certainty in structural prediction. To guarantee both sequence reliability and structural integrity, our selection threshold was set at a minimum score of 90.

2) Non-toxicity. The peptides passing the primary filter were subsequently subjected to toxicity prediction using the ToxinPred2.0 online platform (https://webs.iiitd.edu.in/raghava/toxinpred2/batch.html). This step was critical for identifying and removing any sequences with potential toxic properties, allowing only those predicted to be non-toxic to proceed.

3) Non-allergenicity. The resulting non-toxic subset was further analyzed for potential immune responses using the AlgPred 2.0 server (https://webs.iiitd.edu.in/raghava/algpred2/batch.html). The objective of this final filter was to eliminate peptides with predicted immunogenic activity, thereby refining our candidate pool to those with a higher likelihood of being safe for subsequent wet-lab studies.

2.4 Structure Verification for the De Novo Predicted Sequences

In total, 22 potential PSP were identified through screening; their characteristics are detailed below (Table S7). For precise structural identification of these 22 candidate peptides, we utilized our group's established parallel peptide synthesis platform[1] to prepare authentic standards for all predicted sequences. To obtain synthetic peptide standards with native C-terminal carboxylic acid moieties, we evaluated several compatible solid-phase synthesis resins: 2-Chlorotrityl chloride, Wang, MBH-Br[5], and 4-MeO-BH-Br[6] resins, all of which produce the desired C-terminus upon cleavage. Following comprehensive evaluation of reaction kinetics, resin cost, and final product purity, 2-Chlorotrityl chloride resin was selected as the optimal solid support for parallel synthesis of all peptide standards[1].

The synthetic standard mixture was analyzed under the same UPLC–MS/MS conditions applied to the original pangolin scale hydrolysate. Structural confirmation was achieved

through retention-time matching and comparison of MS/MS spectra. Detailed comparison data are presented below, including: (1) retention-time deviation to assess chromatographic repeatability, (2) cosine similarity to quantify MS/MS spectral match quality (Table S7), and (3) mirror and scatter plots of b/y-ion intensities to visualize spectral congruence. Representative results are shown in Figures S5–12.

Table S7 Detailed information for the predicted de novo sequencing with structure verification

No.	Peptides[A]	De novo score	Allergenicity/Toxicity	RT1[B] (min) de novo	RT2[C] (min) standard reference	ΔRT[D] (min)	Cosine similarity
1	NSFFPR	99	NO	58.56	58.61	0.05	0.9813
2	VVSAAHCYK	99	NO	8.11	10.45	2.34	0.9904
3	FPSLVGR	99	NO	63.98	65.92	1.94	0.9971
4	FSLPR	98	NO	32.10	31.84	0.26	0.9953
5	PAPPKPEPR	98	NO	8.01	9.44	1.43	0.9991
6	VSLNAAK	97	NO	8.99	11.09	2.10	0.9895
7	PAPPKGPEPK	97	NO	7.79	9.04	1.25	0.9312
8	VGRPEPGPR	96	NO	7.98	9.10	1.12	0.9980
9	Ac-KATVSLPR	96	NO	32.67	30.96	1.71	0.9814
10	YHKPSVF	96	NO	21.26	20.54	0.72	0.9844
11	GYGVSLPR	95	NO	39.84	41.79	1.95	0.9426
12	YGGLQVR	94	NO	25.69	27.21	1.52	0.9051
13	LPRPKY	94	NO	19.37	21.00	1.63	0.9997
14	Ac-KCSQLNVNCKG	98	NO	19.48	19.80	0.32	0.9851
15	Ac-KAFTAPR	91	NO	31.21	30.52	0.69	0.9227
16	KNPGVYTK	90	NO	7.58	9.16	1.58	0.9921
17	SSGSSGYPVTLR	90	NO	46.47	46.01	0.46	0.9656
18	LNSFFPR	99	NO	116.68	118.91	2.23	0.8257

19	Ac-KLTHPNFN	98	NO	37.13	37.43	0.30	0.8254
20	KLATPAR	97	NO	7.82	9.05	1.23	0.8680
21	Ac-KVSLQVR	93	NO	40.44	40.87	0.43	0.8923
22	VATVSLYR	92	NO	39.28	38.64	0.64	0.8747

[A] Ac- means acetylation on the *N*-termini, and reductive alkylation by iodoacetamide (carbamidomethylation) was carried out for all sample pretreatment before UPLC-MS/MS analysis.

[B] RT1 is the retention time for specific de novo sequencing peptide using nano UPLC-MS/MS.

[C] RT2 is the retention time for standard reference peptide from parallel synthesis using nano UPLC-MS/MS.

[D] ΔRT is the absolute value of [RT1 – RT2].

Although a retention time shift (ΔRT) up to 2 min (Table S7) appears relatively large for conventional liquid chromatography systems, this deviation is analytically acceptable for peptide identification in the current investigation due to the implementation of nano UHPLC with the total analysis time up to 131 min. The nano UHPLC setup functions at an ultra-low flow rate of 0.3 μL/min, representing roughly 1/3300th of the flow rate in conventional HPLC systems (typically 1 mL/min). Given these parameters, merely 0.6 μL of mobile phase (0.3 μL/min × 2 min) traverses the column—a quantity inadequate to disrupt peptide adsorption onto the stationary phase. Furthermore, the intrinsic heterogeneity of the natural peptide sample could also play a role in retention time fluctuations. Possible intermolecular interactions among co-eluting peptides, such as transient hydrophobic binding or charge-based effects, might alter elution dynamics and lead to slight variations in retention times[7]. Furthermore, the observed retention time deviation of 2 min represents less than 2% of the total analytical duration (131 min), a minimal fraction that substantiates the analytical robustness of our approach. This minor deviation, considered alongside aforementioned nano UHPLC flow rate analysis, collectively confirms the high accuracy of PSP de novo sequencing.

Representative structural verification data, including mirror and scatter plots, are presented in Figures S5–12.

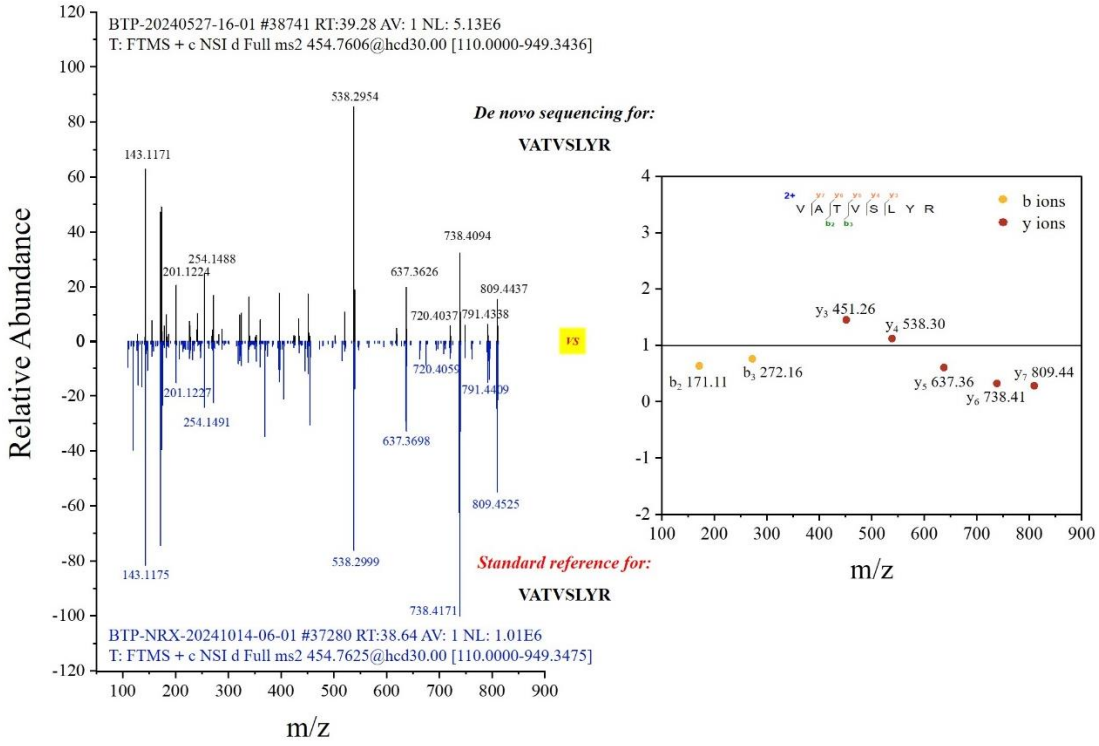

Fig. S5. Structure verification for VATVSLYR.

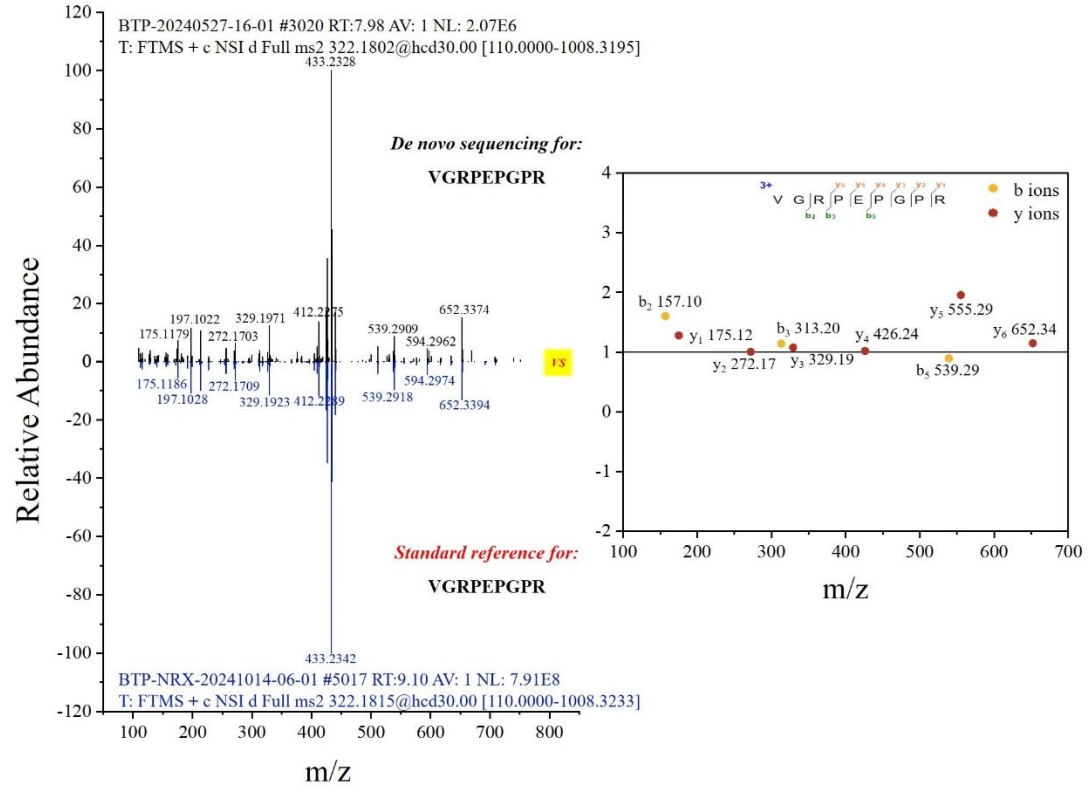

Fig. S6. Structure verification for VGRPEPGPR.

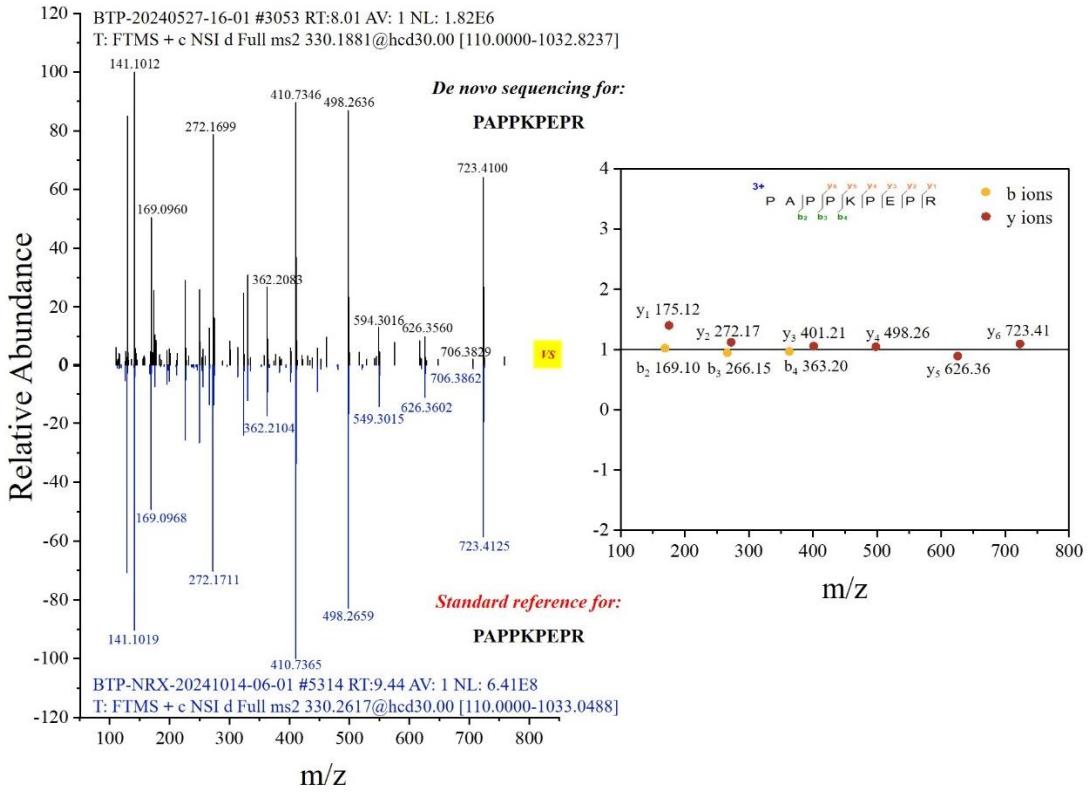

Fig. S7. Structure verification for PAPPKPEPR.

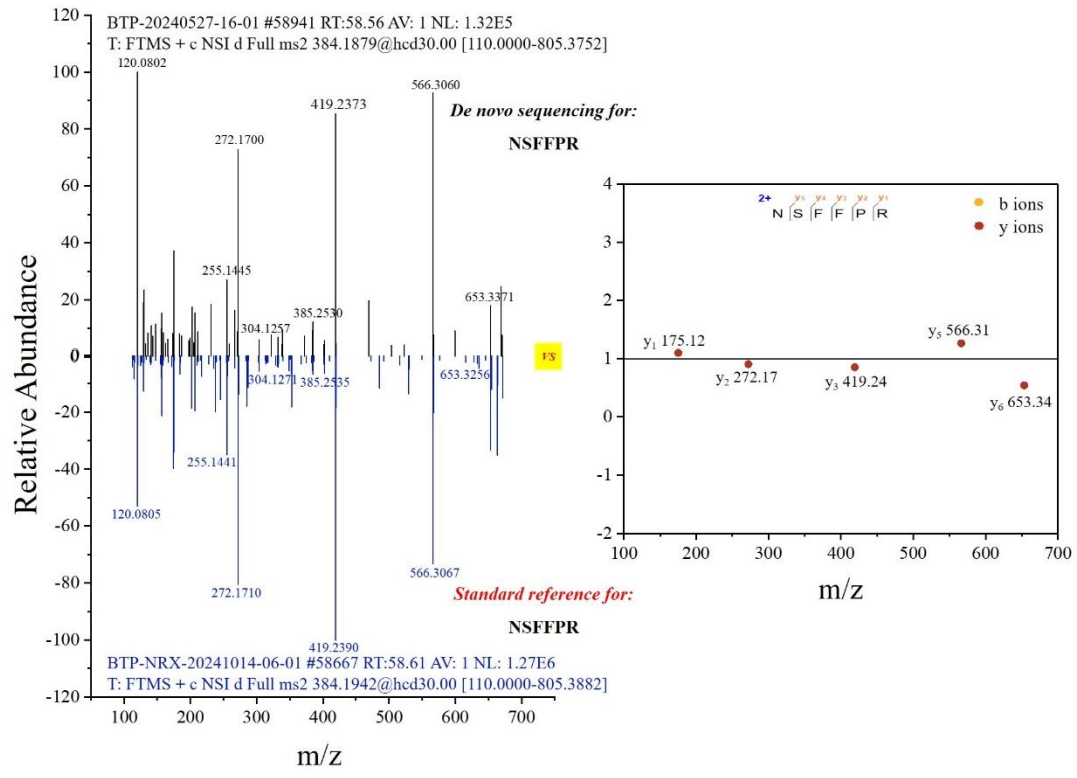

Fig. S8. Structure verification for NSFFPR.

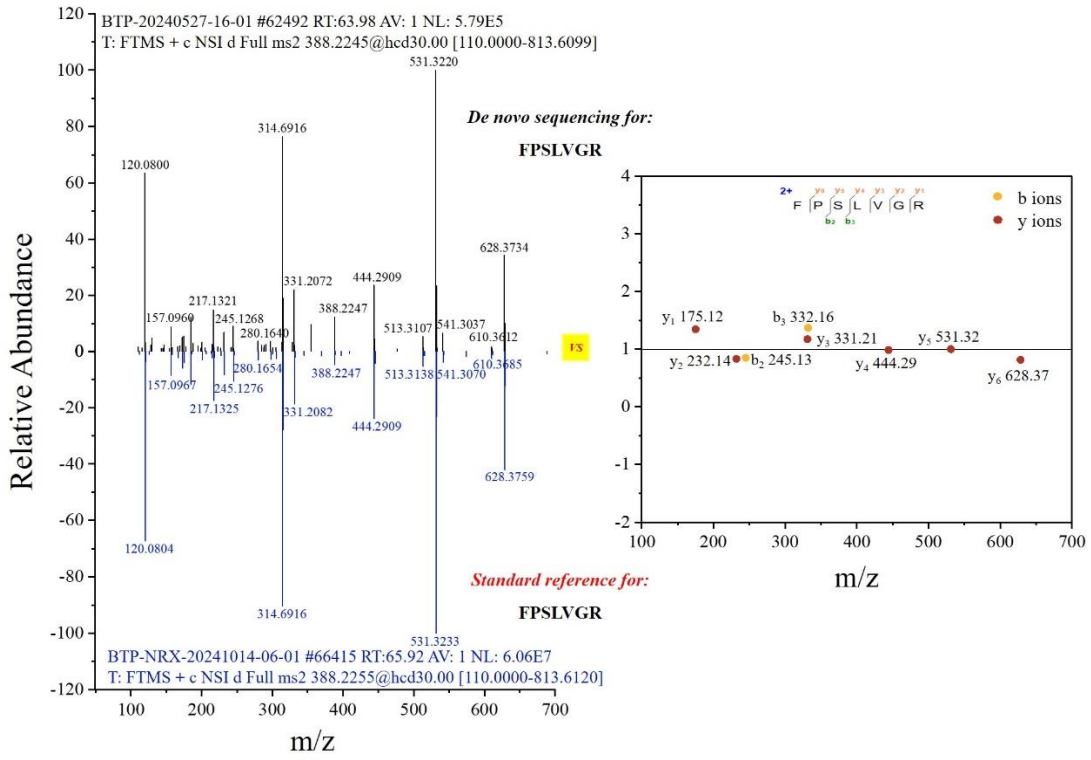

Fig. S9. Structure verification for FPSLVGR.

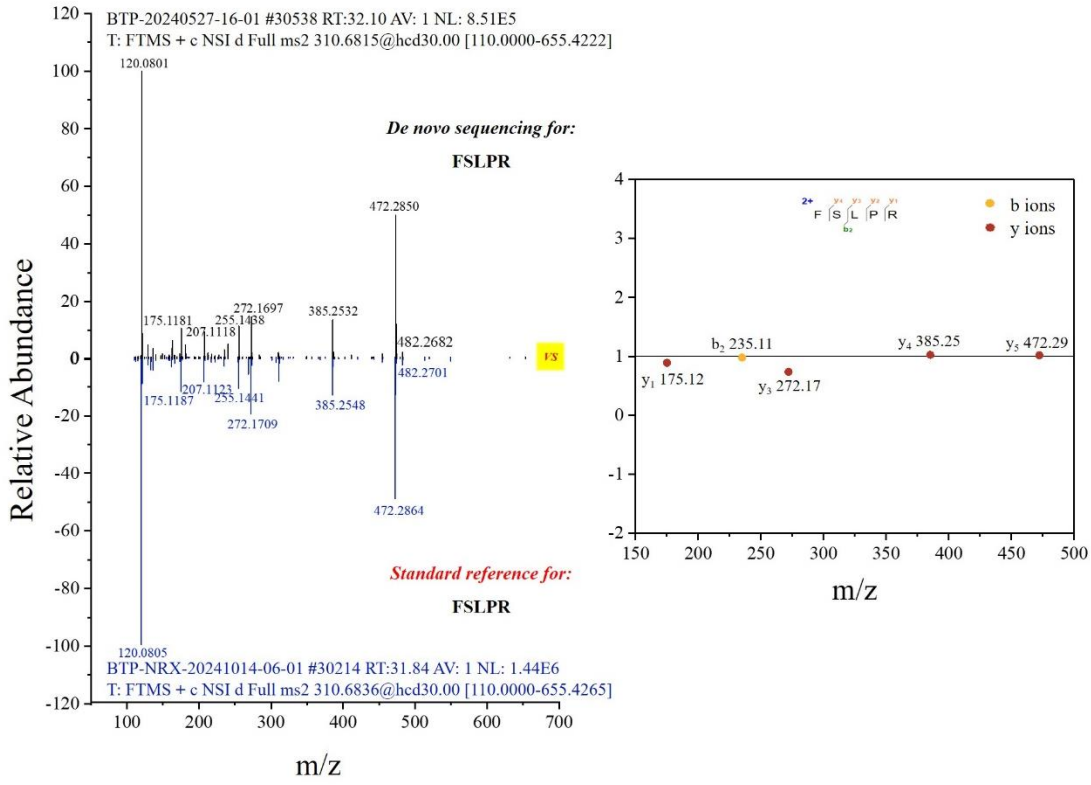

Fig. S10. Structure verification for FSLPR.

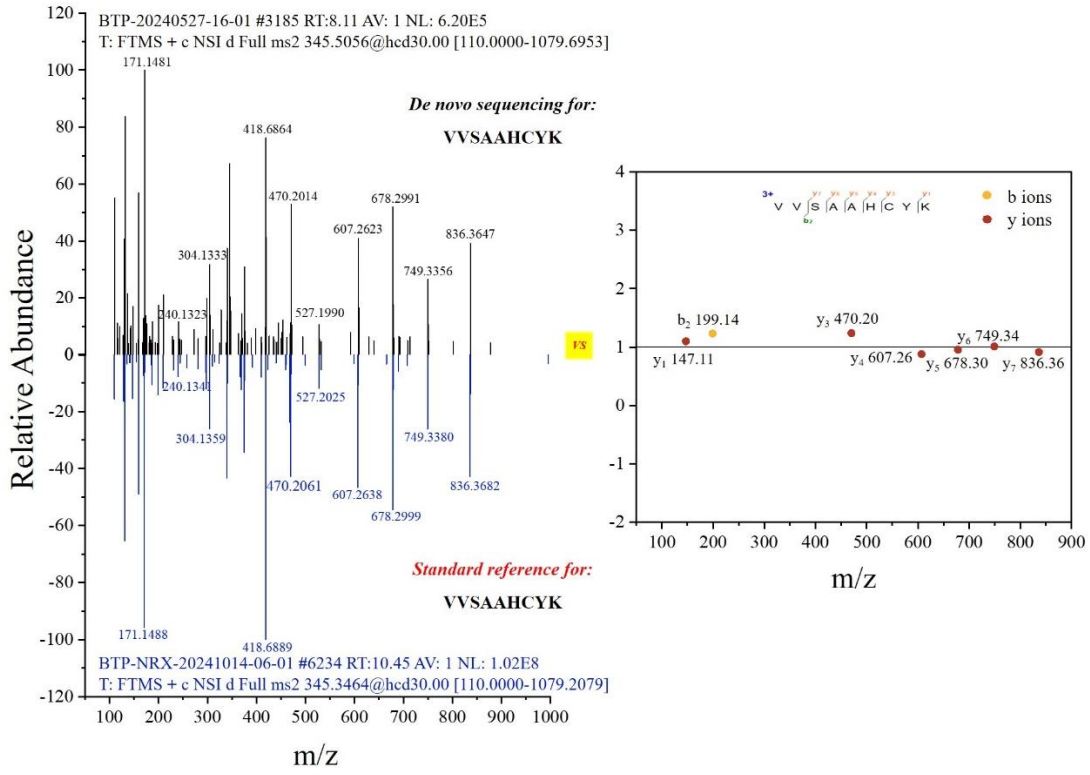

Fig. S11. Structure verification for VVSAAHCYK.

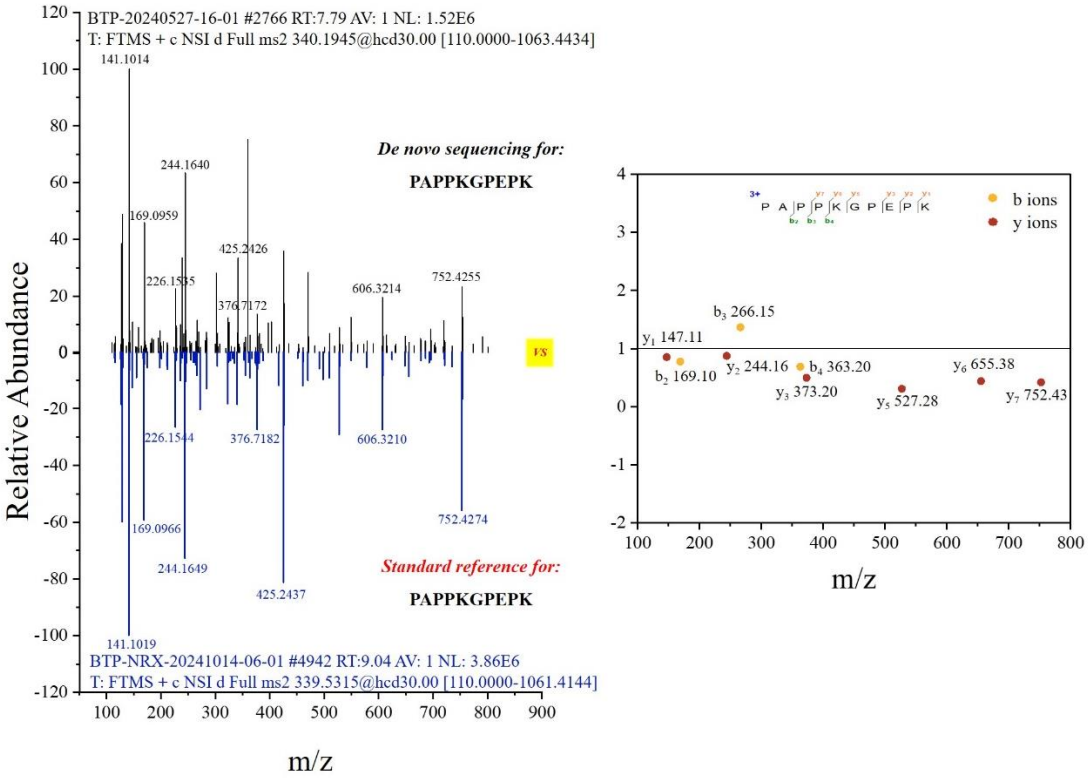

Fig. S12. Structure verification for PAPPKGPEPK.

2.5 Proof for the Existence of Free Cysteine (-SH) by the Use of Different Antioxidant Assays

Table S8 In vitro antioxidant activity of different PSP

No.	Peptides	DPPH assay[A] (%)	ABTS assay[B] (%)	Iron Reduction Assay[C]
1	NSFFPR	11.25 ± 0.22	18.14 ± 1.44	0.018 ± 0.004
2	VVSAAHCYK	69.00 ± 0.03	96.90 ± 0.14	0.197 ± 0.002
3	FPSLVGR	15.73 ± 2.11	26.37 ± 0.68	0.021 ± 0.008
4	FSLPR	10.94 ± 1.30	20.38 ± 1.21	0.016 ± 0.016
5	PAPPKPEPR	13.65 ± 1.26	13.57 ± 0.09	0.003 ± 0.008
6	VSLNAAK	55.10 ± 0.00	9.46 ± 1.70	0.005 ± 0.006
7	PAPPKGPEPK	22.22 ± 0.85	7.34 ± 0.34	0.006 ± 0.006
8	VGRPEPGPR	23.13 ± 1.14	4.43 ± 0.84	0.001 ± 0.002
9	Ac-KATVSLPR	11.84 ± 1.29	19.71 ± 3.07	0.008 ± 0.008
10	YHKPSVF	20.78 ± 1.76	92.75 ± 0.19	0.006 ± 0.004
11	GYGVSLPR	15.61 ± 0.48	92.56 ± 0.11	0.023 ± 0.014
12	YGGLQVR	15.06 ± 0.73	92.68 ± 0.24	0.024 ± 0.004
13	LPRPKY	28.96 ± 1.88	94.63 ± 0.10	0.019 ± 0.006
14	Ac-KCSQLNVNCKG	92.19 ± 0.27	95.84 ± 0.34	0.361 ± 0.033
15	Ac-KAFTAPR	34.21 ± 1.36	7.27 ± 2.82	0.023 ± 0.006
16	KNPGVYTK	15.24 ± 0.58	93.02 ± 0.21	0.023 ± 0.006
17	SSGSSGYPVTLR	10.15 ± 1.47	92.68 ± 0.25	0.016 ± 0.007
18	LNSFFPR	46.39 ± 0.27	94.84 ± 0.16	0.060 ± 0.010
19	Ac-KLTHPNFN	54.88 ± 0.66	7.51 ± 0.78	0.014 ± 0.011
20	KLATPAR	10.84 ± 0.94	24.89 ± 3.60	0.025 ± 0.007

21	Ac-KVSLQVR	11.05 ± 1.46	27.21 ± 2.28	0.010 ± 0.008
22	VATVSLYR	21.48 ± 0.67	93.93 ± 0.05	0.022 ± 0.013

[A] DPPH radical scavenging activity was given here with the use of corresponding peptide at 1 mM concentration.

[B] ABTS radical scavenging activity was given here with the use of corresponding peptide at 0.5 mM concentration.

[C] Iron reduction capacity was given here with the use of corresponding peptide at 0.2 mM concentration.

2.6 In vivo Evaluation of the Antioxidant Activity and Associated Phenotypes of PSPA Gel in C. elegans

2.6.1 Stress Resistance Evaluation

Table S9 Average and maximum lifespan of C. elegans under oxidative stress

Group	Mean lifespan (h)	Percentage increase (%)	Maximum lifespan (h)	Percentage increase (%)
Control	3.36 ± 0.20	—	6.67 ± 0.58	—
PSPA gel	4.06 ± 0.10**	20.86	8.67 ± 0.58*	29.99

Data are presented as mean ± SD from three independent experiments. $^{*}p < 0.05$, $^{**}p < 0.01$ relative to control.

Table S10 Average and maximum lifespan of C. elegans under heat stress

Group	Mean lifespan (h)	Percentage increase (%)	Maximum lifespan (h)	Percentage increase (%)
Control	3.18 ± 0.18	—	6.67 ± 0.58	—
PSPA gel	4.91 ± 0.26***	54.40	8.33 ± 0.58*	24.89

Data are presented as mean ± SD from three independent experiments. $^{*}p < 0.05$, $^{***}p < 0.005$ relative to control.

2.6.2 Activation of Endogenous Antioxidant Defense System

Table S11 Effect of PSPA gel on the activity of antioxidant enzymes and malondialdehyde content in *C. elegans*

Group	Dose	Antioxidant enzyme activity [A]			MDA content [B]
		SOD	CAT	GSH-Px	
Control	0 μM	94.68 ± 13.56	69.97 ± 2.99	71.88 ± 13.47	1.19 ± 0.12
PSPA	200 μM	316.90 ± 32.44***	190.60 ± 3.75****	265.30 ± 14.16***	0.42 ± 0.02***

[A] SOD, U/mg prot, CAT, U/mg prot, GSH-Px, U/mg prot.

[B] MDA, nmoL/mg prot.

$^{***}p < 0.005$, $^{****}p < 0.001$

2.6.3 HRMS for the FITC Labeled PSPA (FITC-PSPA)

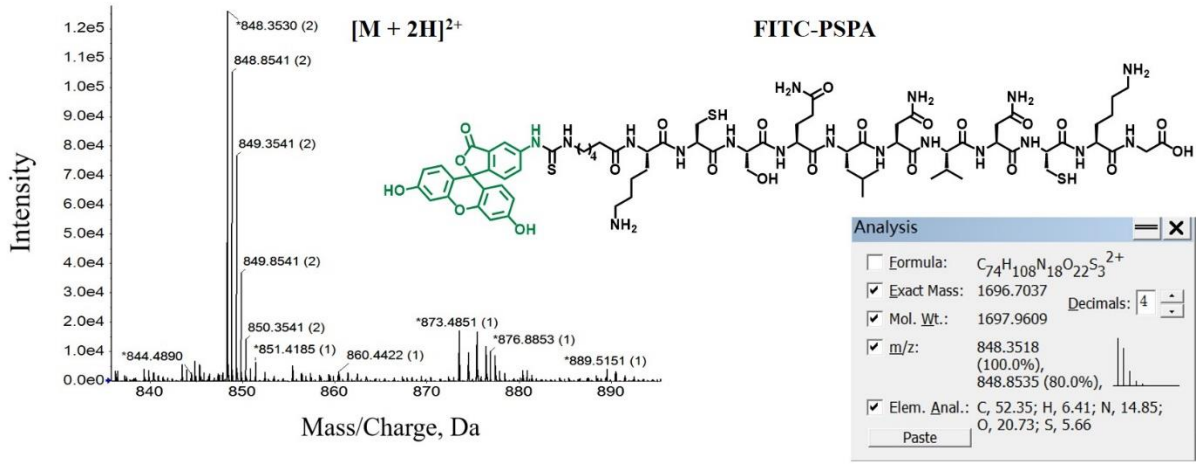

Fig. S13. HRMS for the FITC-PSPA and the predicted HRMS spectrum by ChemDraw software.

2.7 The pH-Dependent Gelation of PSPA Assemblies

To investigate the pH-dependent gelation behavior, PSPA peptide solutions (10 mM) were prepared across a broad pH range (2, 4, 6, 7, 9, and 11) and allowed to equilibrate under ambient conditions. Stable, non-flowing hydrogels were observed to form only within an intermediate pH window (approximately pH 4–9). Under extreme pH conditions (i.e., strongly acidic pH 2 and strongly alkaline pH 11), the samples remained turbid, free-flowing solutions without observable gelation, even after prolonged incubation (Fig. S14). These results indicate that the self-assembly and gelation behavior of PSPA are strongly pH-dependent, with effective gel formation occurring only within a near-neutral pH region.

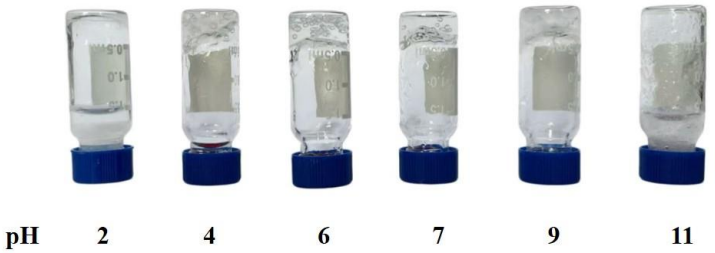

Fig. S14. The pH-dependent gelation of PSPA assemblies.

At low pH (e.g., pH 2), lysine residues (K1 and K10) are expected to be fully protonated (-NH_3^+), while the C-terminal carboxyl group is predominantly protonated (-COOH). Under these conditions, the peptide likely carries a high net positive charge, leading to strong

electrostatic repulsion between molecules. Such repulsion may hinder the close molecular packing required for β-sheet formation and subsequent supramolecular assembly. Furthermore, extensive protonation may disrupt intermolecular hydrogen bonding, thereby weakening the noncovalent interactions required for gelation.

At high pH (e.g., pH 11), several factors may contribute to the loss of gelation. Lysine side chains are expected to be largely deprotonated ($-NH_2$), while cysteine thiol groups (pKa ≈ 8.3) are predominantly deprotonated to thiolate anions ($-S^-$). This shift in ionization state likely alters the overall charge distribution of the peptide and may introduce electrostatic repulsion, thereby disfavoring ordered β-sheet assembly. Moreover, thiolate species are more prone to oxidation under alkaline conditions, potentially leading to disulfide bond formation and interfering with the dynamic noncovalent interactions required for reversible self-assembly. These combined effects may suppress the formation of a stable supramolecular network.

Therefore, the intermediate pH range (4–9) likely represents a balanced condition in which electrostatic interactions are moderated and thiol groups remain in a less reactive state, allowing β-sheet-driven self-assembly to proceed effectively. Notably, this pH window encompasses the physiological range (e.g., pH 7.4), suggesting compatibility of the PSPA assembly system with biologically relevant environments.

2.8 Determination of the Critical Gelation Concentration (CGC) of PSPA Assemblies

To determine the CGC, a series of PSPA solutions were prepared at pH 6 and incubated at room temperature. Peptide concentrations ranged from 0.8 to 1.2 wt%. After equilibration for 24 h, gel formation was evaluated using the standard vial inversion method. The results showed that stable, non-flowing hydrogels formed only at concentrations of ≥1.1 wt%, whereas samples below this threshold remained free-flowing solutions (Fig. S15). Therefore, the CGC of the PSPA system under these conditions was determined to be 1.1 wt%.

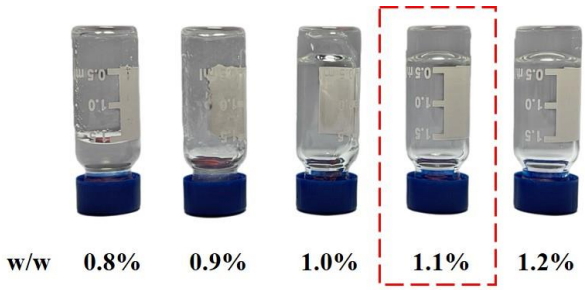

Fig. S15. Determination of the CGC of PSPA assemblies.

These results indicate that PSPA can undergo efficient self-assembly to form a stable supramolecular network at relatively low concentrations, further demonstrating its strong gelation capability.

2.9 Determination of the Mechanical Strength of PSPA Gel

To quantitatively assess the mechanical properties, a strain amplitude sweep was performed on a fully equilibrated PSPA hydrogel (prepared at 10 mM in a pH 6 solution) using a rotational rheometer. The storage modulus (G') and loss modulus (G″) were recorded as functions of oscillatory shear strain (γ), ranging from 0.01% to 100%, at a fixed angular frequency of 10 rad/s and a temperature of 25 °C.

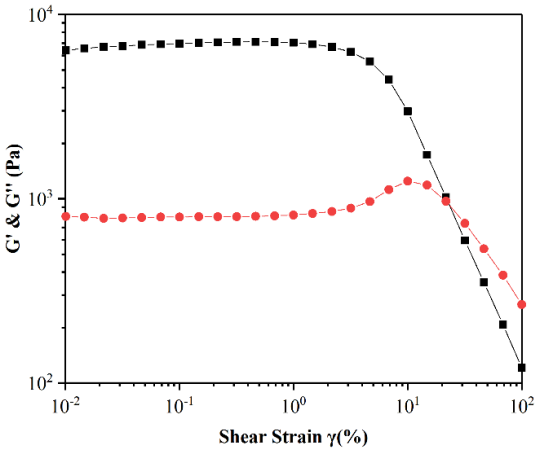

Fig. S16. Strain dependence of G' (black) and G″ (red) for the PSPA gel.

The results reveal a well-defined linear viscoelastic region (LVR) spanning approximately 0.01–2% strain, within which both G′ and G″ remain essentially constant (Fig. S16). Within this LVR, the storage modulus (G′) is approximately 6840 Pa and remains significantly higher than the loss modulus (G″), indicating predominantly elastic, solid-like behavior under small deformations.

As the applied strain exceeds the LVR, both G′ and G″ decrease progressively, reflecting gradual disruption of the supramolecular network. A crossover point (G′ = G″) is observed at approximately 21.7% strain, which can be interpreted as the yielding point of the hydrogel, corresponding to a transition from solid-like to liquid-like behavior.

These results demonstrate that the PSPA hydrogel exhibits well-defined viscoelasticity, maintains a stable network under small deformations, and possesses moderate resistance to mechanical stress, all of which are desirable attributes for potential biomedical applications.

2.10 Rheological Analysis of PSPA Gel

Two rheological measurements were performed on equilibrated PSPA hydrogels (prepared at 10 mM in a pH 6 solution).

First, a steady shear rate-dependent viscosity test was performed over a range of 0.1–100 s^{-1} at 25 °C. The viscosity decreased continuously with increasing shear rate, demonstrating pronounced shear-thinning behavior (Fig. S17). This behavior indicates that the hydrogel can readily flow under applied shear stress, a key prerequisite for injectability.

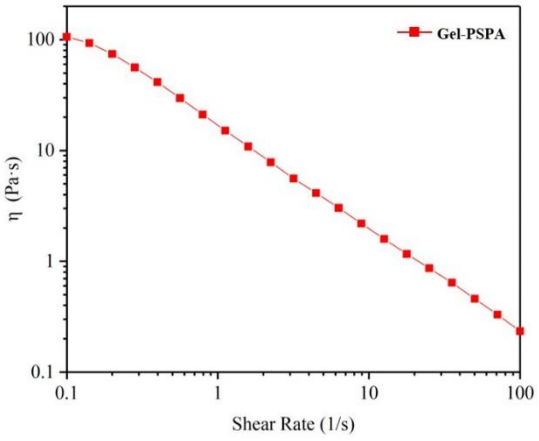

Fig. S17. Steady shear rheology showing viscosity as a function of shear rate.

Second, to evaluate thixotropy and structural recovery, step-strain measurements were performed at a fixed angular frequency (10 rad/s) by alternately applying low strain (γ = 0.1%, within the linear viscoelastic region) and high strain (γ = 100%, beyond the LVR). Under low strain, G′ remained significantly higher than G″, indicating a stable gel-like state. Upon application of high strain, G′ decreased sharply and became lower than G″, reflecting disruption of the supramolecular network and a transition to a sol-like state. Notably, when the strain was

reduced back to the low level, both moduli rapidly recovered to their original values (Fig. S18). This behavior was reproducible over multiple cycles, indicating efficient and reversible network reconstruction after shear-induced disruption.

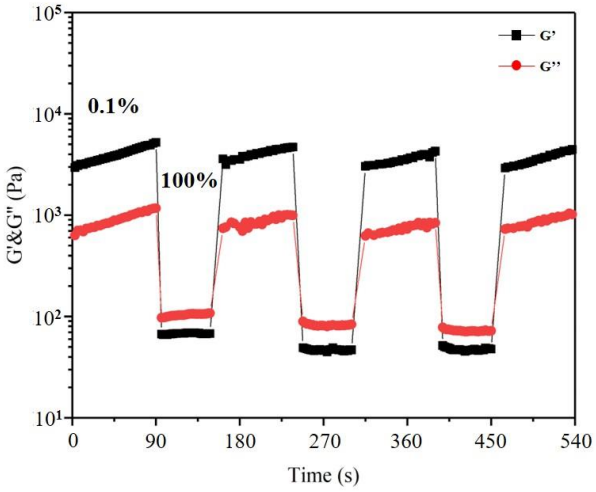

Fig. S18. Step-strain measurements demonstrating thixotropic recovery behavior of the PSPA hydrogel.

These results demonstrate that the PSPA hydrogel exhibits pronounced shear-thinning behavior together with rapid and repeatable structural recovery, characteristics of thixotropic supramolecular systems.

2.11 Stability of PSPA Gel under Physiological Conditions over Extended Periods

To simulate physiological conditions, PSPA assemblies were incubated in phosphate-buffered saline (PBS, pH 7.4) at 37 °C. Samples were collected at defined time points and analyzed using complementary approaches spanning macroscopic to nanoscale levels.

1) Macroscopic Gel Integrity (Vial Inversion Test):

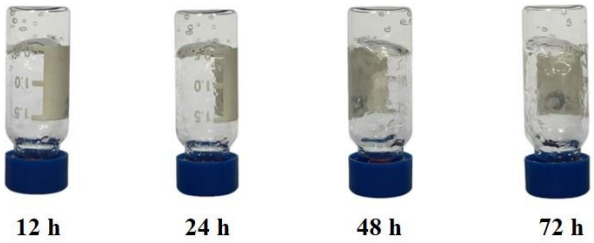

Fig. S19. Stability of the PSPA gel under physiological conditions over extended periods.

The PSPA hydrogel remained non-flowing upon inversion throughout 72 h of incubation in

PBS without added oxidants, indicating preserved macroscopic integrity (Fig. S19). This observation suggests that the assembly is stable under physiological conditions while retaining responsiveness to oxidative stimuli, as evidenced by rapid disassembly upon H_2O_2 treatment (manuscript, page 20, Fig. 6B). Therefore, the system is not inert but exhibits conditional stability, remaining stable under physiological conditions while responding to oxidative environments.

2) Rheological Stability (Time-Dependent Storage Modulus):

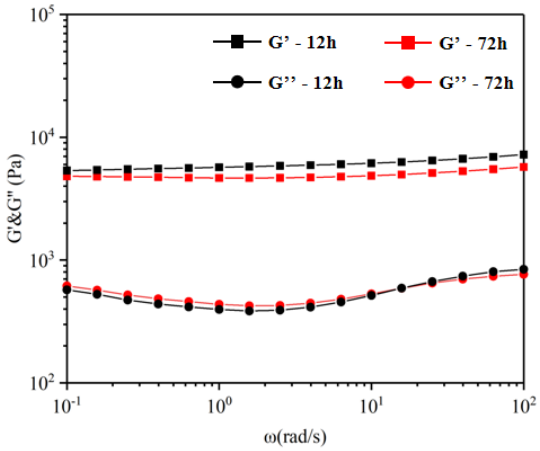

Fig. S20. Rheological stability of the PSPA gel under physiological conditions at 12 h and 72 h time points.

To quantitatively evaluate mechanical stability, rheological measurements (rotational rheometer, 1% strain, 25 °C, frequency sweep 0.1–100 rad/s) were performed on hydrogels incubated for 12 and 72 h. The storage modulus (G′) remained largely unchanged between the two time points (Fig. S20), indicating that the hydrogel maintained stable mechanical strength and network structure under physiological conditions. These results confirm the stability of the viscoelastic properties.

3) Nanoscale Morphological Stability (Scanning Electron Microscopy, SEM):

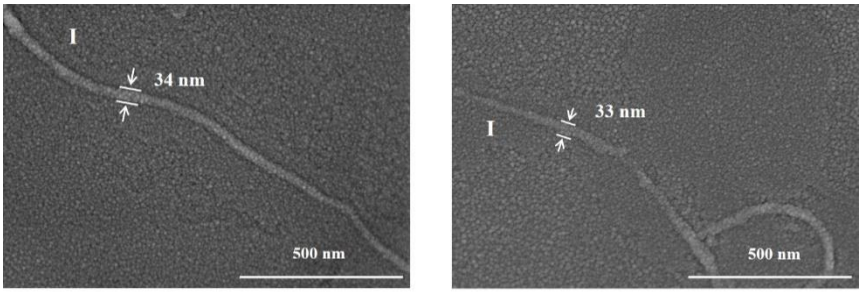

12 h 72 h

Fig. S21. Nanoscale morphological stability of the PSPA gel under physiological conditions at 12 h and 72 h time points.

To assess the stability of the fundamental building block (Filament I), the same sample preparation and imaging conditions as those used in Fig. 5H of the main manuscript were employed. SEM analysis at 12 and 72 h showed that Filament I retained its well-defined nanofibrous morphology with consistent dimensions and architecture (Fig. S21), confirming nanoscale structural stability of the supramolecular network under physiological conditions.

2.12 Cytotoxicity of PSPA Assemblies in HEK293T and RAW 264.7 Cell Lines

To systematically evaluate the biocompatibility of PSPA assemblies, two additional cell lines were selected: HEK293T (a human embryonic kidney-derived normal cell line) and RAW 264.7 (a murine macrophage cell line). These models were selected to assess both general cytocompatibility and potential immunological interactions. Cytotoxicity was evaluated using the same CCK-8 protocol applied to HepG2 cells (manuscript, Fig. 8D), at both identical (20 μM) and higher (100 μM) concentrations to ensure consistency and comparability.

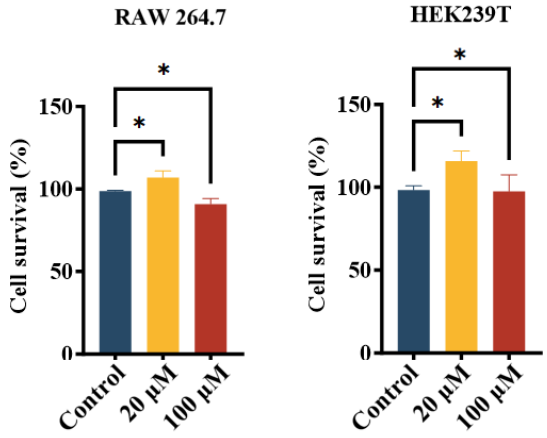

Fig. S22. Cytotoxicity of PSPA assemblies in HEK293T and RAW 264.7 cell lines.

The results show that the peptide exhibits negligible cytotoxicity in HEK293T cells, with high cell viability maintained at all tested concentrations (Fig. S22). As a non-cancerous cell line, HEK293T cells are generally more sensitive to external stimuli than tumor-derived HepG2 cells. Therefore, the observed low toxicity in HEK293T cells provides strong evidence for the intrinsic biocompatibility of PSPA assemblies in normal cellular contexts. Furthermore, inclusion of a kidney-derived cell model expands the evaluation beyond hepatic systems,

indicating that the low cytotoxicity is not tissue-specific.

Cytotoxicity assays in RAW 264.7 macrophages similarly demonstrated minimal adverse effects, indicating that PSPA assemblies do not induce significant cytotoxic responses in immune-related cells (Fig. S22). This finding suggests a favorable immunocompatibility profile, which is particularly relevant for potential biomedical applications of supramolecular peptide assemblies.

Taken together, these results consistently demonstrate low cytotoxicity of PSPA assemblies across multiple cell types (tumor, normal, and immune) and over a broader concentration range (up to 100 μM), providing a robust and general assessment of their biosafety.

Reference:

[1] Y. M. Li, S. F. Gao, X. H. Zhang, Z. Cao, Y. Y. Guo, R. K. Zhao, Y. G. Liu, X. X. Li, H. Y. Lin, Q. Qin, B. Q. Yi, G. D. Zhao, *Food Res. Int.* **2025**, 212, 116475.

[2] P. A. Wender, D. J. Mitchell, K. Pattabiraman, E. T. Pelkey, L. Steinman, J. B. Rothbard, *Proc. Natl. Acad. Sci. U. S. A.* **2000**, 97, 13003.

[3] M. Jullian, A. Hernandez, A. Maurras, K. Puget, M. Amblard, J. Martinez, G. Subra, *Tetrahedron Lett.* **2009**, 50, 260.

[4] N. D. Zaharuddin, I. Barkia, W. Z. W. Ibadullah, M. Zarei, N. Saari, *Int. J. Biol. Macromol.* **2022**, 220, 1512.

[5] M. Leko, P. Filippova, M. Dorosh, K. Rustler, T. Bruckdorfer, S. Burov, *Org. Process Res. Dev.* **2022**, 26, 144.

[6] S. Ficht, R. J. Payne, R. T. Guy, C. H. Wong, *Chem. Eur. J.* **2008**, 14, 3620.

[7] C. T. Mant, Y. Chen, Z. Yan, T. V. Popa, J. M. Kovacs, J. B. Mills, B. P. Tripet, R. S. Hodges, *Methods Mol Biol.* **2007**, 386, 3.